Unleashing the Potential of Rare Earth Ions in modified Calcium Titanate for Strategic Anti-Counterfeiting Application

Synthesis of rare-earth doped $Ca_{(0.9)}Zn_{(0.1)}TiO_3$ phosphor powder

The phosphor materials were prepared using the following precursors: $CaCO_3$ (99.0%), ZnO (99.0%), TiO_2 (99.9%), H_3BO_3 (99.0%), Pr_6O_{11} (99.9%), and Er_2O_3 (99.9%), sourced from Sisco Research Laboratories, India. The precursors were accurately weighed and mixed through grinding in an agate mortar and pestle. Subsequently, pellets were formed using a hydraulic press at 1200 psi and subjected to pre-sintering at 650˚ C for 2 hours. This was followed by sintering at 1350˚ C for 2 hours in an ambient atmosphere using a tubular furnace, with a heating rate of 5°C/min. The sintered pellets were ground to produce the desired phosphor powder for further characterization.

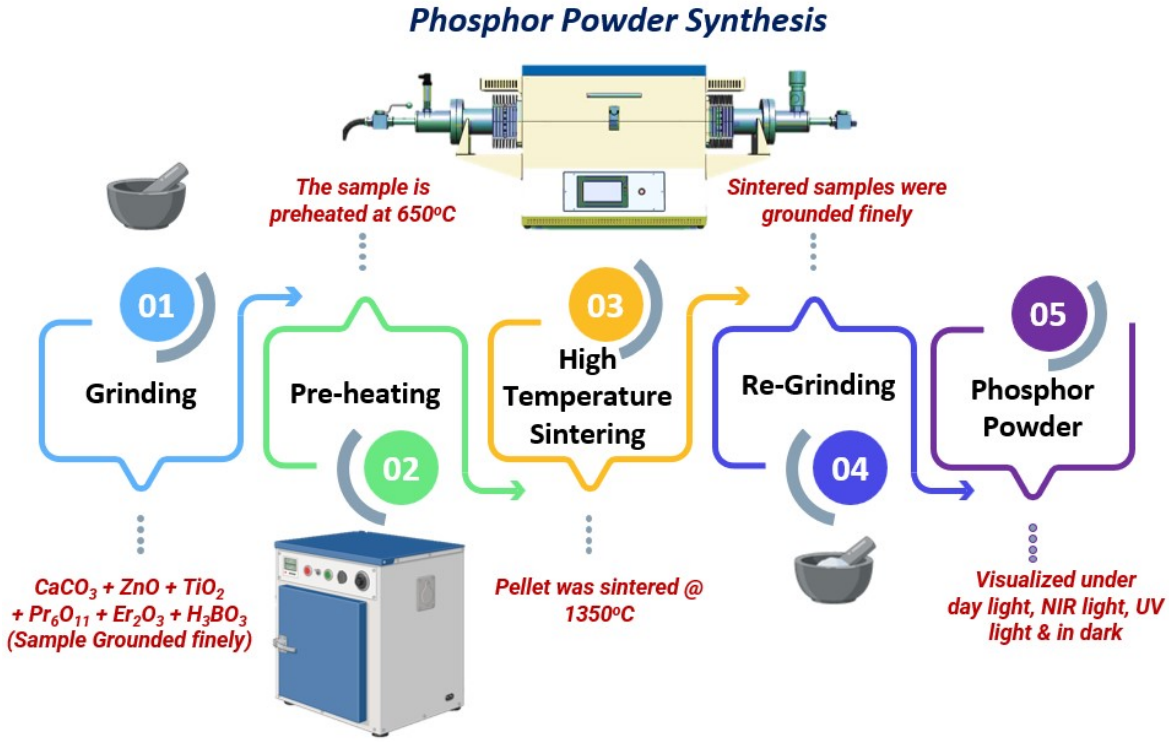

Fig. S1. Schematic representation of steps involved in preparation of Pr^{3+} and Er^{3+} doped $(Ca_{0.9}Zn_{0.1})TiO_3$ phosphor powder

† Footnotes relating to the title and/or authors should appear here.
Supplementary Information available: [details of any supplementary information available should be included here]. See DOI: 10.1039/x0xx00000x

Instruments for Characterization

Powder X-ray diffraction (P-XRD) analysis for all the samples was performed using the Panalytical X-Pert3 diffractometer with CuKα_1 (λ= 1.5406 Å) as source radiation at an operating voltage of 30 kV and current 40 mA. Rietveld refinement for the optimized sample was performed using GSAS II software to evaluate the phase purity of the as-prepared material. The surface morphology and the elemental composition of the optimized phosphor were studied using field emission scanning electron microscopy (FESEM) technique via FEI QUANTA 250 FEG, Thermo Fisher equipped with energy-dispersive X-ray spectroscopy (EDX) feature. Transmission electron microscopy (TEM) images and selected area electron diffraction (SAED) patterns were captured using G2-20 TWIN, FEI –TECNAI operated at acceleration voltage 200 kV. Diffusive reflectance spectroscopy (DRS) of the as-prepared phosphor samples was carried out using UV Vis – NIR spectrophotometer, JASCO V-670. Fourier transform Infra-red spectrophotometer (FTIR) was performed using IRAffinity-1, Shimadzu to study the functional and vibrational groups of the samples. Photoluminescence studies such as room temperature excitation and emission spectra, time-resolved decay characteristics, and up-conversion photoluminescence measurements were analysed using FLS1000 spectrophotometer, Edinburgh Instruments, UK. Internal and external quantum efficiency of the samples was recorded using FP-8550 Jasco spectrofluorometer attached with integrated sphere setup with a bandwidth of 5 nm.

Powder X- Ray diffraction studies

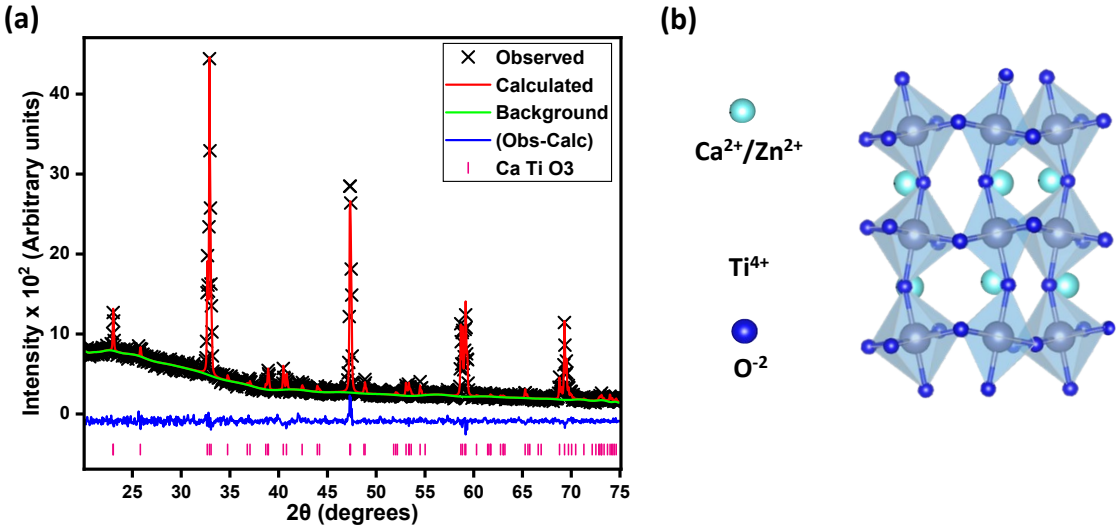

Fig. S2 (a) Rietveld refinement of the optimized sample CZTP: 0.30 mol% Er^{3+}, (b) crystal structure of $(Ca_{0.9}Zn_{0.1})TiO_3$ perovskite structure.

The refinement yielded a χ^2 value of 1.78 and a goodness-of-fit (GOF) value of 1.33, indicating an excellent fit between the observed and calculated diffraction patterns.

Table S1. Lattice parameters obtained from Rietveld refinement.

Sample code	a (Å)	b (Å)	c (Å)	$\alpha=\beta=\gamma$ (°)	Volume (Å^3)	GOF	Reduced χ^2
Undoped $CaTiO_3$	5.37919	5.43704	7.64349	90	223.548	1.13	1.28
CZTP: 0.30 mol% Er^{3+}	5.37758	5.44005	7.63877	90	223.467	1.33	1.78

Field emission scanning electron microscopy and EDAX studies

To visualize and analyse the crystal structure in detail, the crystal structure was designed using the Visualization for Electronic and Structural Analysis-3.0.7 (VESTA) software[1] (The $CaTiO_3$ CIF file is exported from the Materials Project database) as shown in Fig. S2 (b). Detailed visualization of the atomic arrangements and site occupations within the orthorhombic $CaTiO_3$ lattice was observed. The $CaTiO_3$ adopts an orthorhombic perovskite structure and crystallizes in the orthorhombic Pnma space group.[2] In this structure, the Ca^{2+} ions are situated in an 8-coordinate geometry, bonded to eight O^{2-} atoms. The Ca–O bond distances exhibit a range between 2.35 Å and 2.67 Å. The Ti^{4+} ions are coordinated by six O^{2-} atoms, forming TiO_6 octahedra that share corners. The octahedra display tilt angles of 25° relative to one another. The Ti–O bond lengths within the octahedra are slightly asymmetric, with four shorter bonds measuring 1.96 Å and two longer bonds at 1.97 Å.

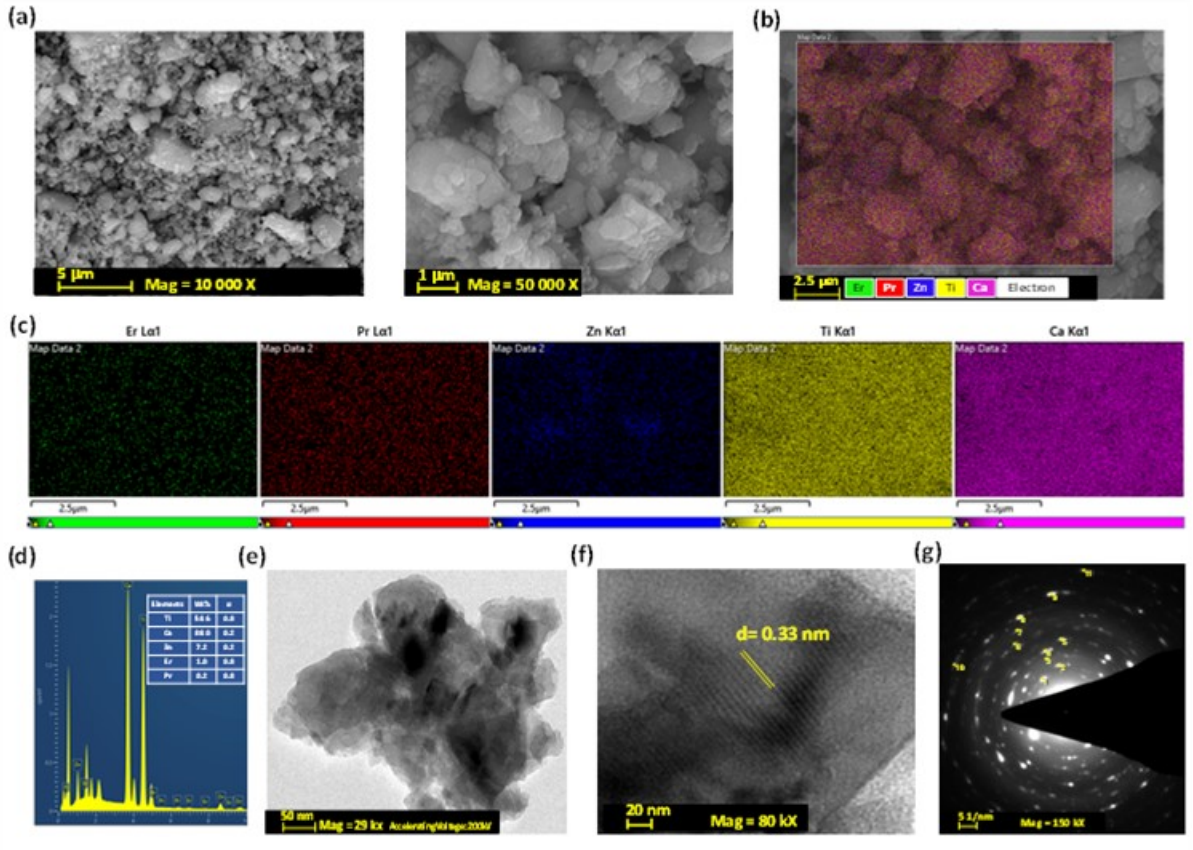

Fig. S3. Morphological analysis of CZTP: 0.30 mol% Er^{3+} phosphor. (a) FE-SEM images, (b) overall EDAX image, (c) Elemental distribution images, (d) and EDAX spectra, (e) TEM image, (f) HR-TEM image, (g) SAED pattern.

Temperature Dependent Photo-Luminescence studies

For any phosphor material, temperature stability is crucial for its practical applications. When a phosphor is exposed to elevated temperatures, it can affect its luminescent properties, such as emission intensity and colour. Moreover, due to thermal quenching effect, temperature dependence of the phosphor is expected to show significant reduction in luminescence intensities. Therefore, for applications such as lighting, displays, or security features, understanding the temperature stability ensures reliable performance over time and environment. Therefore, investigation on luminescence intensity with respect to temperature ranging from 25 deg to 175 deg at excitation wavelength of 379

nm was carried out to the optimized sample as shown in Fig. S4 (a). Interestingly, even at high temperature of 100 ˚ C, more than 50 % of total emission intensity was found to be intact, which proves excellent thermal stability of the prepared phosphor material. Also, the relative intensity variations of each emission peaks 613 nm, 533 nm, and 543 nm were shown in Fig. S4 (b). As observed, the Pr^{3+} emission peak at 613 nm showed a monotonic reduction at a faster rate with the increasing temperature whereas the Er^{3+} emission peak at 543 nm showed gradual decrease in intensity. Emission peak at 533 nm from Er^{3+} ions was found to increase with increasing temperature. This could be due to the particle population on respective levels confirming to the Boltzmann distribution.[3] At higher temperature, due to thermal activation an energy transition takes place from $^4S_{3/2}$ to $^2H_{11/2}$ level which also indicated that emission intensity at 533 nm is more favourable with increasing temperature.[4]

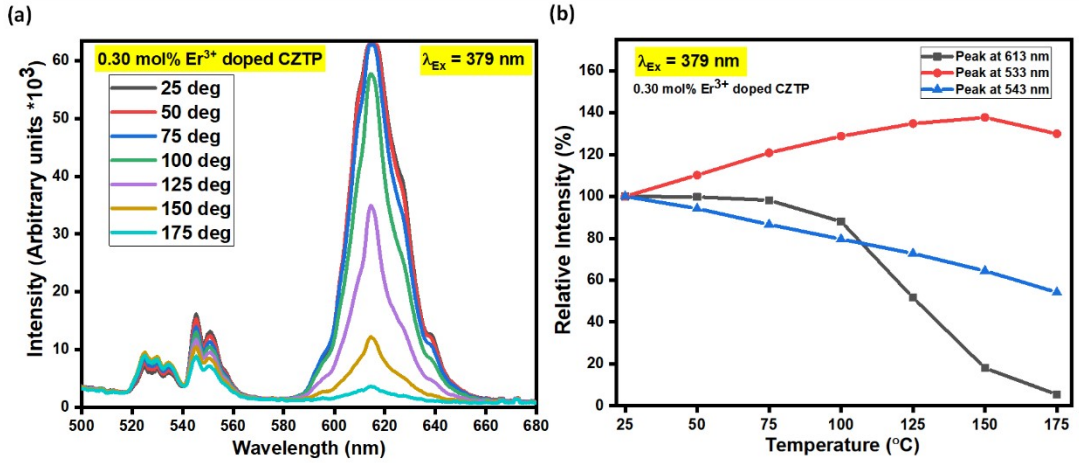

Fig. S4. Temperature dependent photoluminescence analysis (a) TDPL spectra of CZTP: 0.30 mol% Er^{3+} under 379 nm excitation, (b) Intensity of each peak with respect to different temperature.

Time resolved photoluminescence studies

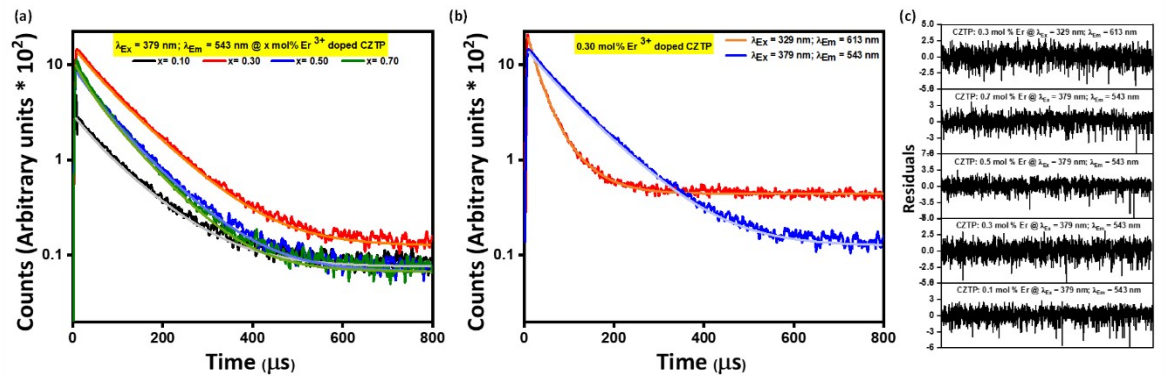

Fig. S5. TRPL decay profile of (a) x mol % Er^{3+} doped CZTP, (b) 0.30 mol % Er^{3+} doped CZTP at different excitation and emission conditions, (c) Residuals of each decay profile fit.

Table S2. TRPL decay fit results for 'x' mol% Er^{3+} doped CZTP samples.

Sample/fit data	τ1 (μs)	τ2 (μs)	A1	Rel %	A2	Rel %	Avg. Lifetime (μs)	χ2
x= 0.1	36.8	98.7	75.6	11.4	219.9	88.6	91.6	1.12
x= 0.3	37.6	95.6	303.1	9.7	1104.7	90.3	90	1.04
x= 0.5	41.6	93.4	335.0	22.0	525.9	77.9	82	1.07
x= 0.7	26.6	81.7	387.2	15.8	670.9	84.2	73	1.10

Table S3. TRPL decay fit results of 0.30 mol% Er^{3+} doped CZTP sample at different excitation and emission wavelengths.

Source/fit data	τ1 (μs)	τ2 (μs)	A1	Rel %	A2	Rel %	Avg. Lifetime (μs)	χ2
Ex = 329 nm, Em = 613 nm	22.4	57	1440.8	36.3	441.5	40.0	37.5	1.07
Ex = 379 nm, Em = 543 nm	37.6	95.6	303.1	9.7	1104.7	90.3	90	1.04

The energy transfer efficiency (η_T) from Pr^{3+} to Er^{3+} ions have been calculated by the using the following equation,

$$\eta_T = \left(1 - \frac{\tau}{\tau_0}\right) \times 100\%$$

Where, τ_0 is the lifetime value of $^1D_2 - {}^3H_4$ state of Pr^{3+} in $(Ca_{0.9},Zn_{0.1})TiO_3$:0.25 mol% Pr^{3+} in the absence of Er^{3+} ions and τ is the lifetime value of the same state in the presence of 0.30 mol% Er^{3+} under excitation wavelength of 379 nm. The average lifetime values of τ and τ0 were found to be 28.5 μs and 34.6 μs respectively from time resolved photoluminescence data. Thus, the obtained energy transfer efficiency was found to be 17.5% for the optimised sample of $(Ca_{0.9},Zn_{0.1})TiO_3$ with 0.30 mol% of Er^{3+} and 0.25 mol% of Pr^{3+}. Table represent the calculated energy transfer efficiency percentage for sample with varying concentration of Er^{3+}. It can be seen from the table S3 and fig 2(c) that as the concentration of Er^{3+} increases, energy transfer efficiency from Pr^{3+} to Er^{3+} ions increase as consequence of which the emission intensity of 543 nm peak escalates, however the emission intensity of 613 nm peak reduces.

Table S4. Energy transfer efficiency of the prepared phosphor materials with varied concentration of Er^{3+} ions.

Sample name	Energy transfer efficiency (%)
CZTP: 0.1 mol% Er^{3+}	1.0
CZTP: 0.3 mol% Er^{3+}	17.5
CZTP: 0.5 mol% Er^{3+}	43.3
CZTP: 0.7 mol% Er^{3+}	50.7

Formulation of anticounterfeiting ink

The choice of dispersion medium/solvent plays a vital role in formulating anticounterfeiting ink and maintaining optical properties.[6] The PVC gold medium serves as a versatile dispersive medium, crucially allowing for uniform dispersion of phosphor powder without cluster formation.[7] Procured commercial PVC gold medium was found to have a viscosity of about ~876 centipoise (cP). It ensures effective adhesion to printing substrates while facilitating efficient ink application. Therefore, the as-prepared phosphor powder was made to be dispersed in PVC gold media solution (50:1 by weight) via probe sonication for about 30 minutes at 45 kHz to obtain a highly homogeneous anticounterfeit ink solution. The resultant solution was used to make various patterns on the porous, semi-porous, and non-porous substrates by using the screen-printing technique.

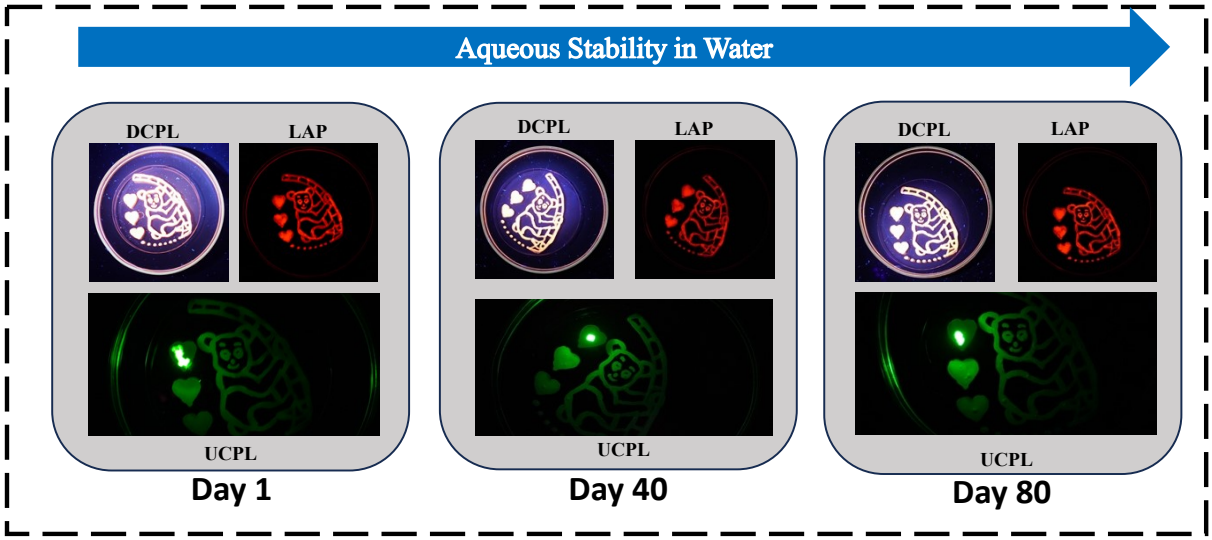

Fig. S6. Aqueous stability test of the phosphor ink deposited glass substrate soaked in DI water.

No degradation in the emission characteristics of the sample was observed even after a time of 3 months, which indicates that the as-prepared ink possesses good aqueous stability as shown in fig. S6.

Spectral parameters

Table S5. Concentration dependent colour purity of the samples.

λ_{Ex} = 379 nm at x mol% of CZTP	CIE Coordinates (x,y)	Color Purity (%)
X = 0.10	(0.555, 0.375)	80
X = 0.30	(0.504, 0.444)	86
X = 0.50	(0.465, 0.481)	85
X = 0.70	(0.429, 0.509)	83
X = 1.10	(0.399, 0.535)	81

Table S6. Excitation wavelength dependent colour purity.

Excitation of 0.30 mol% of CZTP	CIE Coordinates (x,y)	Color Purity (%)
λ_{Ex} = 329 nm	(0.670, 0.324)	99

λ_{Ex} = 379 nm	(0.504, 0.444)	86
λ_{Ex} = 980 nm	(0.259, 0.722)	97

Table S7. Brief summary of literature work on anti-counterfeiting performance of the materials.

S.No.	Phosphor material	Anti-counterfeiting performance	Salient features	Ref
1	La_4GeO_8: Eu^{2+}, Er^{3+}	λ_{ex} = 254 nm emit pink light. λ_{ex} = 365 nm and 980 nm exhibit green emission.	Sample exhibit PL, UCPL. No afterglow was observed.	8
2	$Bi_2Mo_2O_9$:1% Pr^{3+}/1%Er^{3+}	λ_{ex} = 365 nm exhibit faint yellow emission, λ_{ex} = 254 nm emit yellow-white light.	Sample exhibit bright yellow fluorescence at low temperature. No afterglow and up-conversion were reported.	9
3	$Sr_9In(PO_4)_7$: Yb^{3+}, Er^{3+}	Emission colour changes with temperature for λ_{ex} = 980 nm, greenish-yellow shade at room temperature, at 398 K bright green emission and at 573 K a bluish-green shade.	Sample exhibit fluorescence of different colour with increasing temperature conditions.	10
4	$Ba_2Ga_2GeO_7$: Pr^{3+}/Er^{3+}	λ_{ex} = 365 nm exhibit green emission, λ_{ex} = 254 nm exhibit white emission. White persistent luminescence after ceasing 254 nm excitation. Green UCPL under 980 nm excitation.	Sample exhibit PL, UCPL, afterglow luminescence.	11
5	$Na_2CaGe_2O_6$: Pb^{2+}/Er^{3+}	λ_{ex} = 254 nm exhibit blue emission, λ_{ex} = 980 nm green luminescence and green afterglow for 4 s after ceasing 980 nm excitation.	PL, UCPL, short afterglow luminescence (4 seconds).	12
6	$(Ca_{0.9}Zn_{0.1})TiO_3$: Pr^{3+}, Er^{3+}	λ_{ex} = 329 nm and 365 exhibit red emission, long afterglow; λ_{ex} = 379 nm exhibit yellowish green emission; λ_{ex} = 980 nm emit green colour.	PL, long afterglow (12 minutes), UCPL. Excitation dependent and concentration dependent colour tunability are observed.	current work

References:

1 P. Fernández de Cos, .

2 J. Huang, S. Hu, M. Ju and S. Li, *Mater Chem Phys*, 2021, **266**, 124525.

3 J. Xue, H. M. Noh, S. H. Park, B. R. Lee, J. H. Kim and J. H. Jeong, *Journal of the American Ceramic Society*, 2020, **103**, 1174–1186.

4 X. Zhou, L. Ning, J. Qiao, Y. Zhao, P. Xiong and Z. Xia, *Nature Communications 2022 13:1*, 2022, **13**, 1–9.

5 P. Singh, S. Modanwal, H. Mishra and S. B. Rai, *Ceram Int*, 2024, **50**, 32206–32216.

6 P. Kumar, J. Dwivedi and B. K. Gupta, *J Mater Chem C Mater*, 2014, **2**, 10468–10475.

7 C. Dubey, A. Yadav, D. Baloni, S. Singh, A. K. Singh, S. K. Singh and A. K. Singh, *Methods Appl Fluoresc*, 2023, **11**, 025001.

8 P. Pei, R. Wei, B. Wang, J. Su, Z. Zhang and W. Liu, *Adv Funct Mater*, 2021, **31**, 2102479.

9 N. Zhu, Y. Huang, L. Lang, X. Yang, L. Huang, G. Bai and S. Xu, *J Lumin*, 2022, **251**, 119244.

10 W. Chen, H. Gao, Q. Chen, X. Geng and B. Ma, *Ceram Int*, 2024, **50**, 23256–23263.

11 P. Pei, K. Liu, Z. Ju, R. Wei and W. Liu, *J Mater Chem C Mater*, 2022, **10**, 5240–5248.

12 Z. Sun, J. Yang, L. Huai, W. Wang, Z. Ma, J. Sang, J. Zhang, H. Li, Z. Ci and Y. Wang, *ACS Appl Mater Interfaces*, 2018, **10**, 21451–21457.